The Astrophysical Journal, 693:812–821, 2009 March 1 doi:10.1088/0004-637X/693/1/812

SOLAR RELEASE TIMES OF ENERGETIC PARTICLES IN GROUND-LEVEL EVENTS

Donald V. Reames
Institute for Physical Science and Technology, University of Maryland, College Park, MD 20742, USA; dvreames@umd.edu
Received 2008 August 18; accepted 2008 November 13; published 2009 March 3

ABSTRACT

We study the onset times of energetic particles of various species and velocities, v, in large solar energetic particle events with sufficiently hard spectra that are seen by neutron monitors at ground level. Observations of He, O, and Fe from the *Wind* spacecraft provide especially well-defined sequences of onset times, and data from *IMP-8*, *GOES*, and neutron monitors contribute importantly at higher energies. Plotting onset times versus v^{-1} yields a line with the initial solar particle release (SPR) time as the intercept and the magnetic path length as the slope. We find consistent results for 13 of the 16 ground-level events that occurred from 1994 to 2007, in solar cycle 23. Path lengths vary from 1.1 to 2.2 AU in the 13 events. In *all* of the events, SPR times occur after the onset of the shock wave-induced type II radio emission. Events with well-defined SPR times are found over a wide span of solar longitude, suggesting that all ion species and energies are released together, even far from the source longitude, with no evidence of energy- or rigidity-dependent coronal transport. If the SPR time is converted to a radial distance of the source shock wave from the Sun and plotted against longitude, acceleration for well-connected events is found to begin at 2–4 solar radii over a longitude span of $\sim 100^{\circ}$ and to rise to greater heights only at longitudes more distant from the source, as would be expected from shock-acceleration models.

Key words: acceleration of particles – shock waves – Sun: coronal mass ejections (CMEs) – Sun: flares – Sun: particle emission – Sun: radio radiation

Online-only material: color figures

1. INTRODUCTION

In some of the largest solar energetic particle (SEP) events, GeV ions interact in the Earth's atmosphere to produce sufficient intensities of secondary particles at ground level to be detectible above the background produced by galactic cosmic rays. Seventy such ground-level events (GLEs) have been identified as occurring between 1942 and 2007. Early GLEs were listed and their timing was studied in some detail in the classic paper by Cliver et al. (1982) and later events are listed by Cliver (2006), with the exception of the recent event of 2006 December 13.

GLEs appear to be extreme examples of large "gradual" SEP events in which ions are accelerated by shock waves driven out from the Sun by coronal mass ejections (CMEs) (see reviews Reames 1990, 1995, 1999, 2002; Kahler 1992, 1994, 2001; Gosling 1993; Lee 1997, 2005; Tylka 2001; Tylka et al. 2005). Element abundances in gradual events often reflect those of the ambient corona and solar wind that are accelerated by the shock (e.g., Meyer 1985; Reames 1999). These events are contrasted with "impulsive" SEP events associated with solar flares or jets (e.g., Nitta et al. 2006) characterized by unusual 1000-fold enhancements of ^{3}He/^{4}He and heavy elements (Z > 50)/O (e.g., Reames & Ng 2004) generally believed to result from resonant wave–particle interactions in the turbulent flare plasma (Fisk 1978; Temerin & Roth 1992; Miller & Viñas 1993; Roth & Temerin 1997; Miller 1998). In some large SEP events, however, intermediate abundances may result when remnant suprathermal ions from impulsive events contribute to the seed population accelerated by CME-driven shock waves (Mason et al. 1999; Tylka et al. 2001, 2005; Desai et al. 2003; Tylka & Lee 2006).

GLEs are of more than academic interest to humans since they represent "hard" radiation that can be a significant hazard to astronauts and equipment in space, while secondary neutrons threaten passengers and crew of aircraft on polar routes. Protons of $\sim$ 150 MeV, which are orders of magnitude more intense than those at 1 GeV, can penetrate 20 gm cm^{-2} of Al or 15.5 cm of water and are very difficult to shield. While predicting GLE occurrence in advance remains only a far distant dream, we can certainly improve our understanding of where, when, and how acceleration takes place in these exceptional events.

When GLE onset times were compared with Hα, radio, and X-ray observations in the solar source events (e.g., Cliver et al. 1982), the first relativistic protons were found to be released $\sim$ 5–30 minutes after the earliest photons from the associated flare or radio burst. This is generally taken as further evidence that the particles are accelerated by the shock wave that forms late in the event, when the CME driver of the shock reaches 2 or 3 solar radii (R_S). However, one might also argue that the delay only means that the protons have traveled a longer path length along the magnetic field to Earth. This argument may be tested by studying the onset times of lower-energy particles, which travel the same path length. For example, while relativistic protons travel 1 AU in 9 minutes or 2 AU in 18 minutes, 10 MeV protons, which require at least 57 minutes to travel 1 AU, must take nearly 2 hr to travel a magnetic path length of 2 AU, a time difference that is easily measured. Since the travel time equals the distance divided by the particle velocity, v, a systematic plot of onset time versus v^{-1} has a slope equal to the path length along the magnetic field and an intercept at the earliest solar particle release (SPR) time. Of course, this SPR time defines only the earliest acceleration or release of particles that are unscattered in transit, and provides no information on the duration of the acceleration or release or on the behavior of the more numerous scattered particles that arrive later. This technique has been used for many years to study impulsive SEP events (Lin et al. 1981; Reames et al. 1985) and, more recently, Tylka et al. (2003) used it in a careful study of two impulsive events and three GLEs. For the two impulsive events, the SPR

times occurred precisely at the time of the peak in hard X-rays, while in two of the three GLEs it occurred well after the γ-ray or hard X-ray peaks. For most GLE events, onset timing studies using spacecraft and ground-based data at all energies have not been attempted previously.

Kahler (1994) was the first to interpret SPR times in terms of an altitude above the solar surface where shock acceleration occurs. He plotted the solar source intensities of GLE protons of energies up to 21 GeV against height of the leading edge of the CME, and concluded that maximum acceleration occurred at ~ 5 R_S. However, Kahler used a nominal path length to correct for the proton transit time and did not determine it from observations. This height is consistent with the observed ionization states of energetic Fe ions (e.g., Leske et al. 1995; Tylka et al. 1995), which indicates that Fe is not stripped during or after acceleration, as might be the case in higher density regions of the lower corona (see Ruffolo 1997). Cliver et al. (2004) found that SEP events were much more strongly correlated with type II radio bursts (a proxy for shock waves) beginning at decametric frequencies corresponding ~ 3 R_S than with metric type II bursts with starting frequencies corresponding to ~ 1.5 R_S. More recently, Gopalswamy et al. (2005) studied the CME height at the time of SPR for the GLE events of cycle 23, assuming a fixed path length of 1.2 AU for the particles. They found that acceleration began at heights from 1.4 to 8.7 R_S in 13 GLEs. Thus, a number of lines of evidence suggest that acceleration begins rather high in the corona.

There is considerable evidence that we must consider magnetic path lengths from the Sun to the Earth that exceed the distance along the Parker spiral of ~ 1.2 AU. Magnetic flux tubes have been mapped by tracking the frequency and direction of kilometric type III emission by electrons streaming outward (e.g., Reames & Stone 1986). These maps often show large departures from the Parker spiral. Studies of onset timing of impulsive electron events inside magnetic clouds show path lengths varying from ~ 1.2 AU near the center of the cloud to ~ 3 AU at its periphery (Larson et al. 1997). These studies measure the flux rope topology of the twisting of the magnetic field about the cloud axis. In general, there can be little doubt that CMEs distort the interplanetary field enough to force newly accelerated particles to follow paths considerably greater than 1.2 AU.

In this paper, we undertake a systematic examination of SPR times in GLE events that occurred during the period from 1994 November to 2008 January that was observed by the *Wind* spacecraft. This covers all of solar cycle 23. SEP data from *IMP-8* and the NOAA *GOES* spacecraft and from neutron monitors were also used. Apart from their intrinsic interest, GLE events also provide high intensities of relativistic protons that define the earliest arrival times. These are combined with the accurate measurements of onset times made at lower energies. This significantly extends the study done by Tylka et al. (2003).

2. SOURCES OF SEP ONSET DATA

The first particles of a given velocity to arrive at Earth from a source near the Sun are unscattered particles focused in a narrow cone about the magnetic field. As time increases, greater numbers of particles arrive in a wider cone of pitch angles as the intensity rises and then flattens toward a time of maximum. The measured onset time depends upon the sensitivity of an instrument to particles of that velocity and the levels of pre-event and instrument-specific background. Pitch-angle scattering slows the rise in intensity and delays the apparent onset, a process that has been modeled for large SEP events (Sáiz et al. 2005; see also Ng et al. 2003). Scattering will be discussed below.

For most SEP instruments flown in the last 40 years, measurements of each particle, e.g., pulse heights, must be telemetered to the ground for accurate determination of the particle species and velocity, usually with complex priority systems to insure that species other than protons are sampled. The limited bandwidth for this transmission, typically ~ 1 particle s^{-1}, greatly reduces the effective sensitivity of the instrument when the rates onboard reach 10^3 or 10^4 s^{-1}. Furthermore, high-energy particles that arrive early are more efficiently sampled than low-energy particles that arrive later when they must compete for telemetry space.

A primary source of SEP timing data for this paper is the Low-Energy Matrix Telescope (LEMT) in the Energetic Particles Acceleration, Composition, and Transport (EPACT) experiment on the *Wind* spacecraft (von Rosenvinge et al. 1995). LEMT is a large-geometry (51 cm^2 sr) instrument in which incident particles are identified and binned by species and energy onboard the spacecraft at rates up to $\sim 36{,}000$ particles s^{-1}. The procedure for onboard analysis is described in some detail and sample pulse-height data are shown by Reames et al. (2001), together with particle angular distributions in some of the GLEs we study here. This procedure ensures that each particle is detected with full instrument sensitivity, independent of energy and species, over the full instrument range from ~ 2 to ~ 20 MeV amu^{-1}.

We use the Goddard Medium Energy (GME) experiment on the *IMP-8* spacecraft (e.g., McGuire et al. 1986) for onset times for protons from ~ 4 to ~ 230 MeV. Pulse-height data from this instrument were sampled and analyzed on the ground. The *IMP-8* instrument also provides high-quality electron (3.6–14.5 MeV) data, but we have not included these data in the determination of SPR times, since the identity of sources of electrons and ions is not assured. We intend to examine the electron data separately.

Instruments on the *GOES* spacecraft are not designed for precise energy measurement but as long-term radiation monitors. The Energetic Particle Sensor (EPS) measures proton intensities from 0.4–500 MeV, using solid-state detectors (without anticoincidence) behind various thicknesses of absorber so that the effective geometry factors are a complex function of energy. Differential energy channels obtained by subtraction are not pure and all channels have onsets at nearly the same time. The High Energy Proton and Alpha Detector (HEPAD) combines two silicon surface barrier detectors and a Cerenkov detector to measure protons from 350 to > 700 MeV. The first particles to trigger the higher energy channels of the telescopes, e.g., 400–500 MeV, provide a fairly good high-energy onset time. At ~ 500 MeV, a 20% difference in proton energy implies a difference of only 0.5 min AU^{-1} in v^{-1}. We obtained data from the *GOES 8*, *10*, and *11* satellites from the Space Physics Interactive Data Resource (SPIDR) web site (http://spidr.ngdc.noaa.gov) where instrument descriptions and a discussion of limitations may also be found.

For the largest GLE events, neutron monitor data provides a precise onset time for relativistic protons. The entire network must be examined to find the monitor where the asymptotic arrival direction of the protons lies along the magnetic field direction toward the Sun. However, for many GLE events where the signal is only $\sim 10\%$ or less of the

galactic cosmic ray background, the onset is not well determined since only the peak intensity is seen above background. For some of these cases, the high-energy spacecraft data, with lower background, provide earlier onsets than the neutron monitors. Neutron monitor data are available from several web sites (http://data.aad.gov.au/aadc/gle/ and http://neutronm.bartol.udel.edu/, and other sites referenced thereon). Also, Gopalswamy et al. (2005) summarized onset times at Oulu for most of our events. In most cases, we have used well-analyzed published neutron monitor data cited below.

3. SEP ONSET TIMES

The progression of the SEP onset times at different energies is best illustrated by normalizing the intensities to the pre-event background. LEMT data are shown in Figure 1 for the GLE event of 1998 May 6. The pre-event background is negligible for the higher energy channels of O and Fe, so these channels are normalized rather arbitrarily (near the 1-particle intensity value) so that these can be clearly distinguished visually. For He, the intensities rise rapidly to levels of 2–3 orders of magnitude above background, i.e., the thresholds are ∼ 0.1% of peak intensities. O and Fe also rise rapidly but determination of the onsets is somewhat limited by statistics.

Figure 2 shows LEMT measurements of He, O, and Fe for the large GLE of 2005 January 20. In this case, the pre-event background is extremely high from the previous GLE of January 17. Nevertheless, the huge rise above background makes the onsets clear, especially for Fe where thresholds are again ∼ 0.1% of peak intensities. Note the gentle rise in the background for He after about 0800 UT that is underlined by the lowest energy He channel. This is the result of instrument background, e.g., multiple energetic protons in the telescopes, that comes from the high rates of particles in the instrument during this period. This is a uniform background in the lower left corner of the LEMT pulse-height space (see e.g., Figure 1 of Reames et al. 1997) where some of this background falls onto the He "track" and contributes to the low-energy He channels. No such rise in background is seen for channels of the heavier elements such as O and Fe that are shown; however, the very lowest channel of O and Fe is contaminated and has been omitted. The 2005 January 20 event is the largest in solar cycle 23.

Figure 3 shows LEMT data for the GLE event of 2000 July 14, the well-known "Bastille Day" event. In this event, instrument background strongly affects all He channels so that data cannot be used to determine onsets. However, C (not shown), O, and Fe data define onsets relatively well, since thresholds lie at ∼ 0.01% of peak intensities.

In Figure 4, we show LEMT data for He and O in one of the large "Halloween" events, the GLE of 2003 October 28. The rise in the lowest energy He channel between 1200 and 1400 UT again signals instrument background, but there is a clear time of departure from this background of each of the higher-energy He channels.

Finally, in Figure 5, we show LEMT He data for the 2001 April 18 event. This event shows the power of our technique of normalizing all channels to the pre-event background. The background is extremely complicated in this event. Nevertheless, with the possible exception of the two channels at the lowest energies, we can see the point at which each channel departs from the background. However, the rise of each channel is fairly gradual in this event and the true onset could easily occur

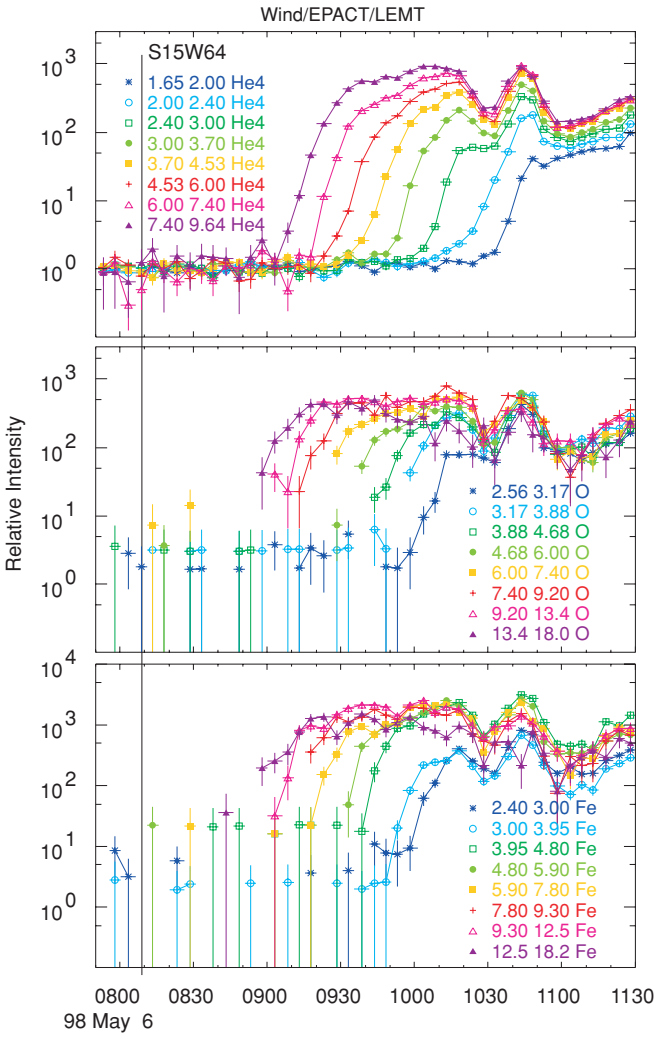

Figure 1. Relative intensities of He, O, and Fe at the listed channels in energy nucleon^{-1} from *Wind*/EPACT/LEMT are shown for the GLE event of 1998 May 6. Where possible, intensities are normalized to the pre-event background in each channel. The pre-event background is negligible for some higher energy channels of O and Fe, so these channels are normalized rather arbitrarily (near the 1-particle intensity value) so that the channels can be clearly distinguished visually.

(A color version of this figure is available in the online journal.)

5–10 minutes earlier than we can measure. This event has the slowest initial rise times we consider.

Figure 6 shows proton data from *IMP-8* in the GLEs of 1998 May 6 and 2002 August 24. Note that background, partially instrumental, continues until 0930 UT in the 4.1–5.96 MeV channel and until 0910 in the 5.96–8.65 MeV channel. Data from the 2002 August 24 event terminate abruptly in a data gap at 0230 UT.

4. SOLAR PARTICLE RELEASE TIMES

Given the onset times of each energy interval determined from figures such as Figures 1–6 above, we determine the velocity, v, corresponding to each interval and plot the onset times against the values of v^{-1} as seen for a sample of events in Figures 7–9. The least-squares fit of a straight line to these points determines the initial SPR time as the intercept and the magnetic path length as the slope. Note again that we do not include electron data in these fits, despite the excellent relativistic electron measurements on *IMP-8*. This is because we do not want to

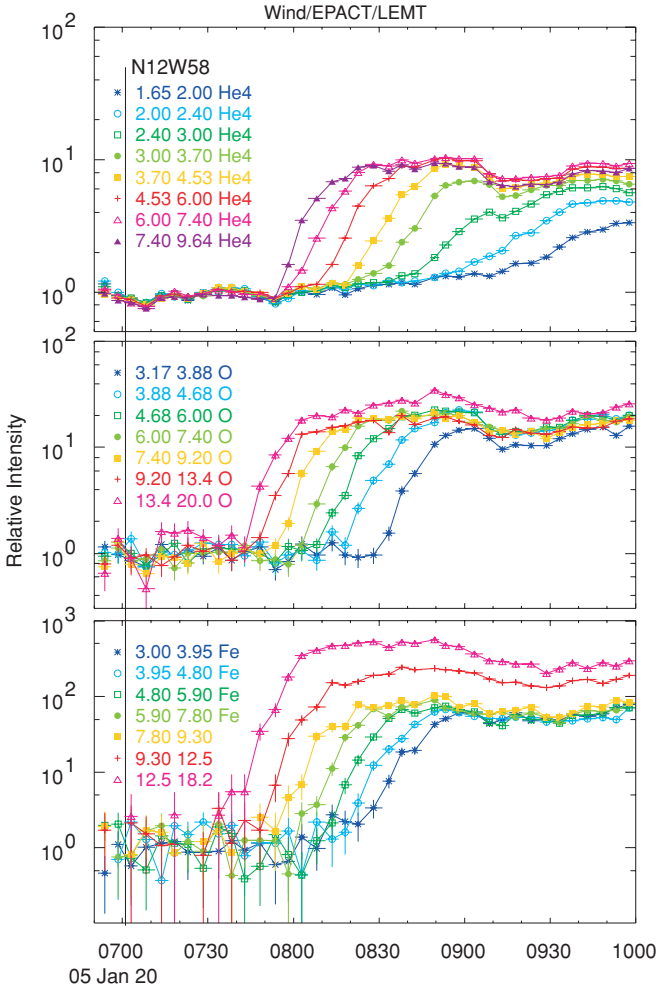

Figure 2. Relative intensities of He, O, and Fe from LEMT are shown for the GLE event of 2005 January 20 normalized as described in Figure 1. This event is the largest GLE in solar cycle 23.

(A color version of this figure is available in the online journal.)

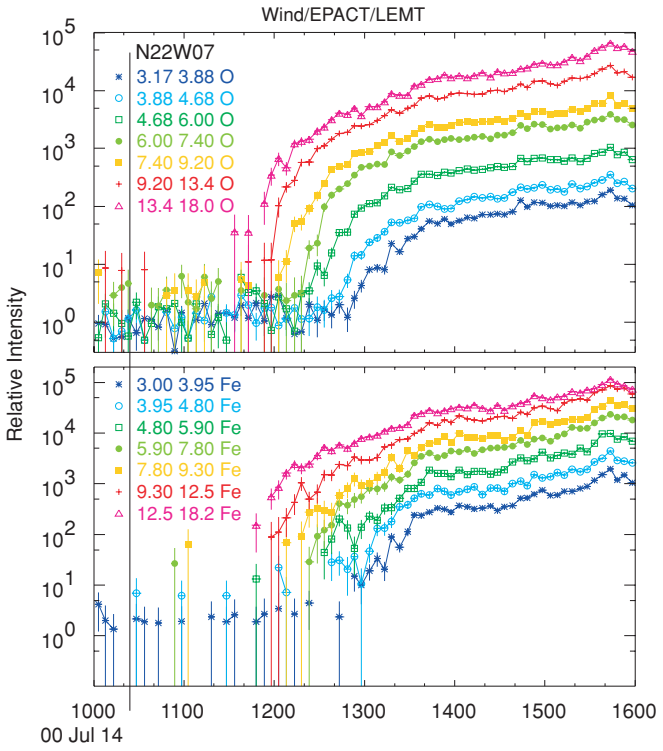

Figure 3. Relative intensities of O and Fe from LEMT are shown for the GLE event of 2000 July 14 normalized as described in Figure 1.

(A color version of this figure is available in the online journal.)

assume, *a priori*, that the electrons are accelerated at the same time and place as the ions, since it is known that electrons are associated with type III bursts, for example, as well as with shock waves (e.g., Krucker et al. 1999; Cliver & Ling 2007).

The upper panel of Figure 7 shows a plot of data from the 1998 May 6 event, corresponding to the temporal plots in Figure 1. This is a clean event with minimal background and high intensities with adequate statistics to provide well-determined onsets. Proton intensities are not so high that they create significant background in the instruments. Measured angular distributions show that pitch-angle scattering of the particles in this event is extremely low (see Reames et al. 2001), and we find that they propagate directly to Earth over a magnetic path length determined to be only 1.11 ± 0.02 AU. Other events may be judged in comparison with this event. If we compare the linear fits for each individual species in this event, initial SPR times for Fe and O, separately, are only 0.9 and 0.7 minutes earlier, respectively, than that for all species together. These are within the 1.6 minutes error quoted on the initial SPR time.

In determining the value of v^{-1} for an interval, we have used the value at the center of the energy interval, even though the first particles will arrive near the top of the interval. The time difference for velocities at the end of an energy interval is comparable with the 5-minutes averaging period and the error we assign to each onset time. Thus, there is some issue of how much of the interval will be filled before the onset becomes detectible. If, instead the whole interval, we assume that only the upper half of the interval must fill so that v^{-1} is determined 75% of the way to the top of the interval, the fitted SPR time for the May 6 event increases by 0.8 minutes. We believe that these uncertainties in the effective values of v^{-1} are tolerable and are well represented by the quoted errors.

By way of comparison, the smaller event of 1998 May 2, also shown in Figure 7, is not nearly as well determined as that of May 6. The intensities are much lower in the May 2 event (see Reames et al. 2001) and the poorer statistics make the onset determination more difficult. Because of the poorer statistics, the onsets for O and Fe are slightly later, on average, than those for He at the same velocity. However, because of a slow intensity rise and background variations in He, we have used all of the species in an attempt to compensate for the scatter in the He onset times.

Figure 8 compares SPR analysis for very large events of 2005 January 20 and 2000 July 14. A data gap allows onset observation of only the highest energy channel of *IMP-8* in the January 20 event, but the LEMT observations in Figure 2 show that He, O, and Fe are well observed. The neutron monitor onset time is extremely well determined (Bieber et al. 2005a; Flückiger et al. 2005; Moraal et al. 2005; Simnett & Roelof 2005). The resultant fit gives a modest path length of 1.19 ± 0.02 AU for this event.

For the event of 2000 July 14, background prevents us from using He onsets, but we compensate by using C, O, and Fe. Neutron monitor onsets are again well determined (e.g., Bieber et al. 2002). For this event, the fit gives a longer path length of 1.71 ± 0.03 in contrast to that in the 2005 January 20 event.

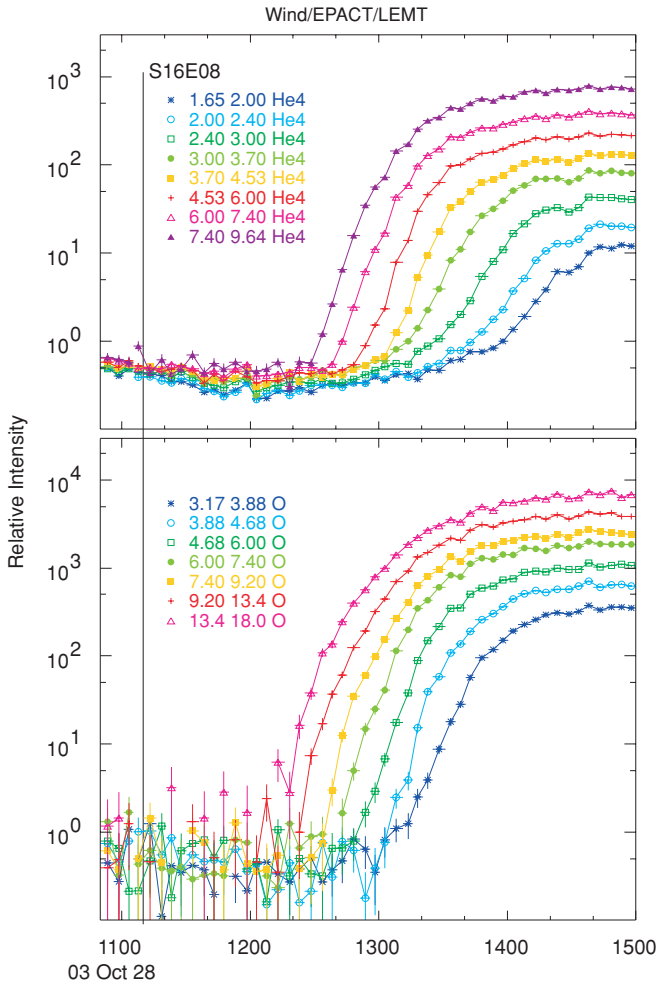

Figure 4. Relative intensities of He and O from LEMT are shown for the GLE event of 2003 October 28 normalized as described in Figure 1.

(A color version of this figure is available in the online journal.)

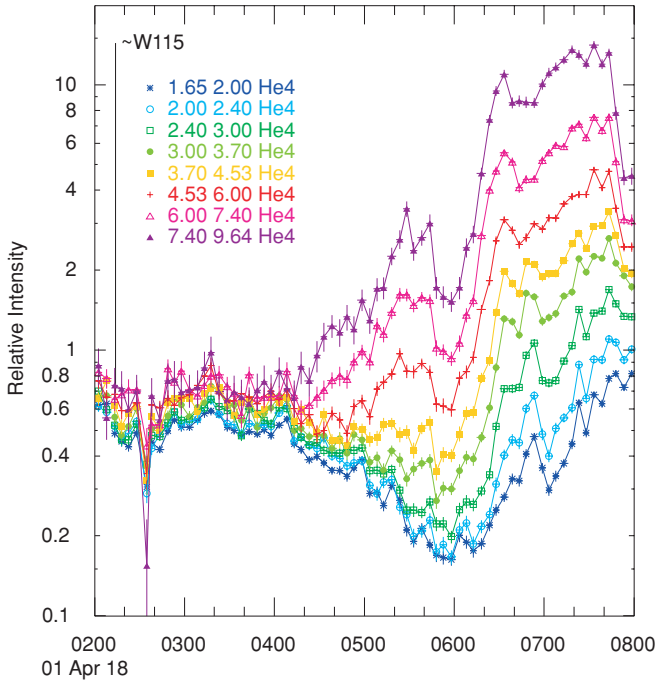

Figure 5. Relative intensities of He from LEMT are shown for the GLE event of 2001 April 18 normalized as described in Figure 1. Onsets for the higher energy channels can be seen despite the complex background.

(A color version of this figure is available in the online journal.)

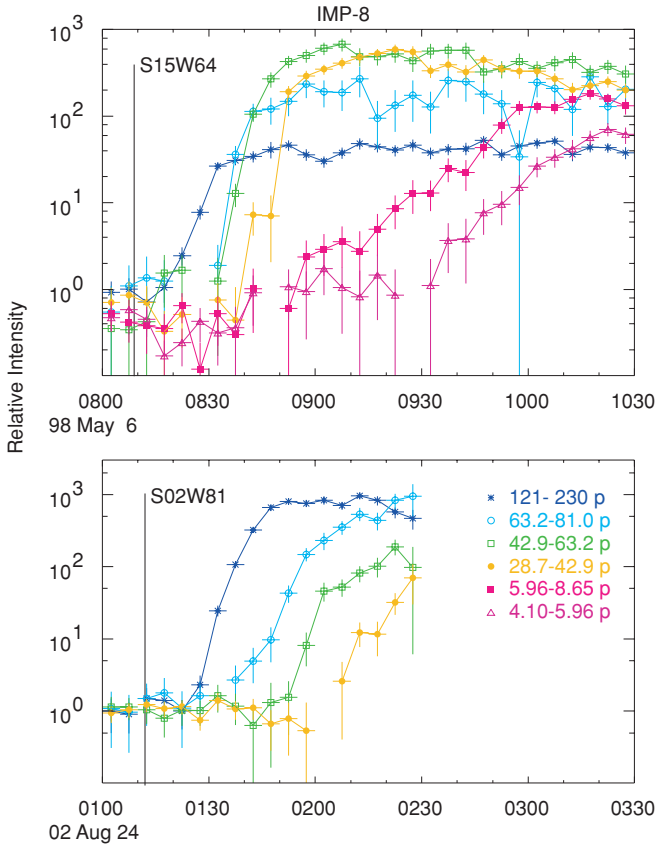

Figure 6. Relative intensities of protons from *IMP-8*, normalized to pre-event background, are shown for the 1998 May 6 and 2002 August 24 GLEs. A data gap begins at 0230 UT in the latter event.

(A color version of this figure is available in the online journal.)

In the upper panel of Figure 9, we show the SPR analysis for the 2003 October event. Neutron monitor data are obtained from Bieber et al. (2005b). For this event, there are no data from *IMP-8*; however, the complete LEMT timing data for He and O, shown in Figure 4, are adequate to complete the SPR analysis.

Our final example is the SPR analysis of the 2002 August 24 event shown in the lower panel of Figure 9. The quality of the *IMP-8* data for this event was shown in the lower panel of Figure 6. This event has the longest path length, 2.16 ± 0.05 AU, in our study. This long path length is already suggested by the extended delay between the onsets of the *IMP-8* channels in Figure 6 where the thresholds are $\sim 0.1\%$ of peak intensities.

In the SPR analysis shown in Figures 7–9, it can be seen that the low-energy data, because of its wide spacing in v^{-1}, is most effective in determining the slope or magnetic path length of an event. The high-energy onset times then determine the SPR time for that path length.

Table 1 lists the initial SPR times and magnetic path lengths that we have been able to determine for 13 of the 16 GLE events in the study period, along with other measured and derived quantities. Individual columns in the table are (1) the GLE number, (2) the initial SPR time, (3) the magnetic path length, (4) the metric type II onset time, from Solar Geophysical Data Bulletins (http://www.ngdc.noaa.gov/stp/SOLAR/sgdintro.html),

Table 1
Solar Release Properties of GLEs

GLE	Initial SPR Time (UT)	Path Length (AU)	Type II Onset (UT)	SPR Type II (min)	Source Location	Vcme (km s^{-1})	*R*(SPR) (sol. radii)
56	98 May 02 1346.7	1.24 ± 0.04	1329.7[(1)]	17.0 ± 2.7	S15W15	938	2.9 ± 0.2
57	98 May 06 0803.5	1.11 ± 0.02	0757.7	5.8 ± 1.6	S15W64	1099	2.0 ± 0.2
58	98 Aug 24 2232.1	1.55 ± 0.04	2153.7	38.4 ± 4.6	N35E09	1275[(2)]	5.7 ± 0.5
59	00 Jul 14 1016.5	1.71 ± 0.03	1008.9	7.6 ± 1.8	N22W07	1674	2.6 ± 0.3
60	01 Apr 15 1347.7	1.59 ± 0.01	1338.7	9.0 ± 1.7	S20W84	1199	2.4 ± 0.2
61	01 Apr 18 0224.3	1.80 ± 0.10	0208.7	15.6 ± 3.2	∼W115	2465	4.8 ± 0.7
63	01 Dec 26 0520.6	1.64 ± 0.06	0503.7	16.9 ± 3.7	N08W54	1446	3.6 ± 0.5
64	02 Aug 24 0100.1	2.16 ± 0.05	0054.7	5.4 ± 2.8	S02W81	1913	2.4 ± 0.5
65	03 Oct 28 1105.1	1.38 ± 0.03	1052.0	13.1 ± 1.8	S16E08	2459	4.3 ± 0.4
66	03 Oct 29 2055.6	1.75 ± 0.09	2031.7	23.9 ± 5.8	S15W02	2029	5.7 ± 1.0
67	03 Nov 02 1713.8	2.01 ± 0.04	1705.7	8.1 ± 2.1	S14W56	2598	3.3 ± 0.5
69	05 Jan 20 0639.5	1.19 ± 0.02	0635.7	3.8 ± 1.2	N12W58	3242	2.6 ± 0.3
70	06 Dec 13 0234.0	1.72 ± 0.05	0218.7	15.3 ± 3.7	S06W26	1774	3.8 ± 0.6

Notes.
[(1)] Type IV onset (metric type II not observed);
[(2)] Shock transit speed (no CME observations).

corrected to the Sun, (5) the SPR time minus the type II onset time at the Sun, (6) the source longitude and latitude (Cliver 2006), (7) the CME speed (Cliver 2006), and (8) the radial distance of the CME-driven shock at the time corresponding to the initial SPR (see below).

Since SPR times refer to times at the Sun, for easy comparison the metric type II onset times in Table 1 are quoted as 8.3 minutes earlier than the time they are observed at Earth. Note that *all SPR times occur after the metric type II onsets*, although several occur only a few minutes after. The lower panel in Figure 10 shows the distribution of initial SPR times as a function of solar longitude. To estimate the location of each CME-driven shock at the time of the initial SPR, we assume a typical metric type II onset frequency of ∼ 100 MHz corresponds to a radius of 1.5 R_S where shock formation begins (e.g., Cliver et al. 2004). This assumption, which covers events where starting frequencies are not given, is probably accurate to ∼ 0.5 R_S for a typical range of starting frequencies (see, e.g., Cliver et al. 2005). Subsequently, the CME speed multiplied by the delay of the SPR time after type II onset gives the height of the shock corresponding to the initial SPR time. The upper panel in Figure 10 shows this location as a function of longitude for each GLE. This plot shows a fairly narrow range of heights, 2–4 R_S, when the observer is reasonably well connected to the source, with heights increasing at the east and west flanks. The algorithm for determining shock height at the time of SPR was chosen to be sufficiently robust allowing future extension to the study of historic GLE events with no CME observations; we examine its accuracy in the next section.

A cartoon showing our understanding of this situation is shown in Figure 11. As the CME drives radially outward from a point near the solar surface, a shock wave forms when the Alfvén speed ahead of the CME falls below the CME speed. The Alfvén speed (and fast-mode speed) decreases rapidly with radial distance to a minimum of ∼ 200 km s^{-1} at ∼ 1.5 R_S (∼ 100 MHz), and rises to a maximum of ∼ 500–700 km s^{-1} at ∼ 3 R_S (∼ 14 MHz) and decreases thereafter (Mann et al. 1999, 2003; Gopalswamy et al. 2001; Vršnak et al. 2002). Thus, it would not be surprising that the fast shocks associated with these GLEs would form near 1.5 R_S and begin to accelerate particles somewhere above 2 R_S. The CMEs encounter this radius and the shocks form over a broad front, depending upon the width of the CME. However, at the flanks of the CME, the shock does not reach more distant longitudes until it expands to much higher altitudes. Thus, we expect the pattern of earliest acceleration, *R*(SPR), against solar longitude that is shown by the red region in Figure 11 corresponding to the pattern in the upper panel of Figure 10. Of course, Figure 11 only begins to approximate the variety of shapes, sizes, and speeds of CMEs and shocks.

5. DISCUSSION

The technique we use to determine a single initial SPR time clearly assumes that particles of all energies were released at a single time and place on the observer's field line, and that there is a single minimum path length that does not change during the transit time of the lowest energy ions. Rapid acceleration of the ions is likely in most SEP acceleration models and, in most cases, a linear fit seems appropriate to the data, as we have shown. As mentioned in the preceding section, differences in the onsets for different species are most likely explained by the poorer statistics of the rarer species.

However, we were unable to find consistent results for three GLE events. The event of 1997 November 6 (at W63) rises very slowly from a declining pre-event background, but a slowly rising instrument background blurs the onsets. The transit of a shock wave from an earlier event near the time of the onsets may further complicate the picture. Tylka et al. (2003) made an SPR analysis of this event using large errors on these measurements, so that the fitted parameters were largely determined by electron data. The event of 2001 November 4 (at W19) shows a small early rise in the high-energy He channels followed by a large rise at later times. The early rise is obscured by background in the lower energy channels and below the statistical thresholds for O and Fe. In the event of 2005 January 17 (at W23), only the peaks from the event are seen above the pre-event background. Note that none of the three events are poorly connected or have atypical source locations.

We believe that a realistic model for the bundle of magnetic field lines near Earth may contain a distribution of paths; some of the field lines may follow a shorter path to a region on the shock and some a longer path to the same or a nearby region. The SPR time corresponds to the shortest path lengths in the distribution, if they are sufficiently numerous. This distribution, with a small number of shorter path lengths and a large number of longer ones, may help us understand the event of 2001 November 4

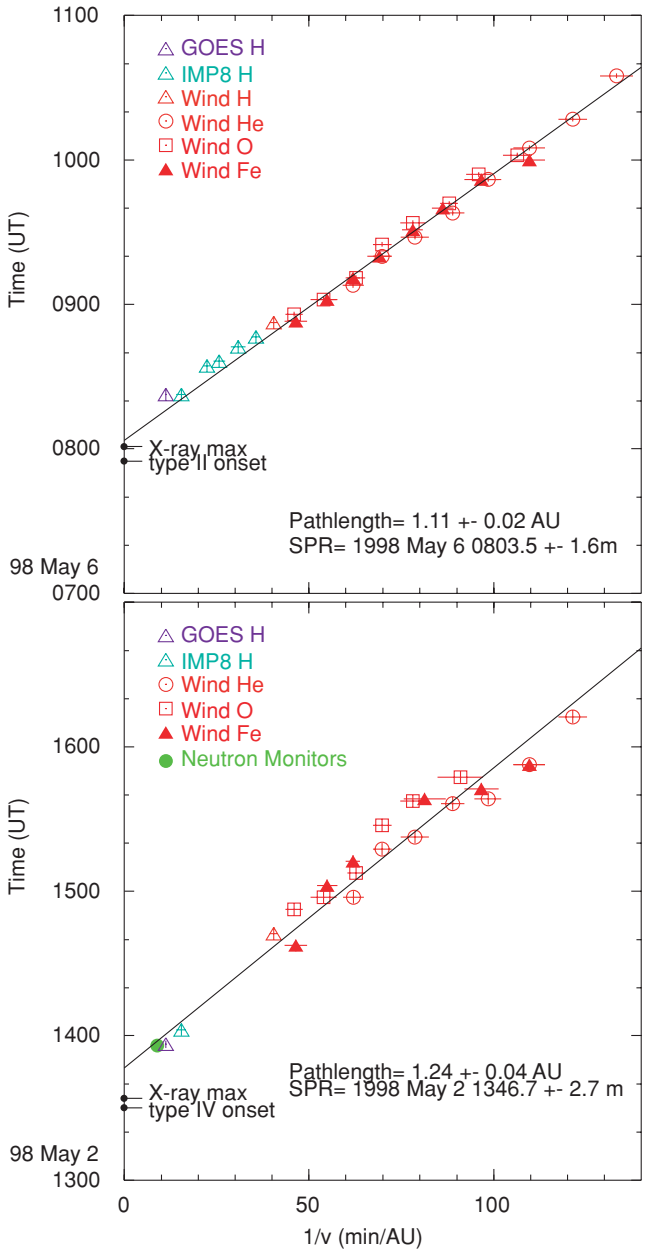

Figure 7. Onset times are plotted against inverse velocity for various energy intervals of listed species. The upper panel is for the GLE event of 1998 May 6 and the lower is for the 1998 May 2.

(A color version of this figure is available in the online journal.)

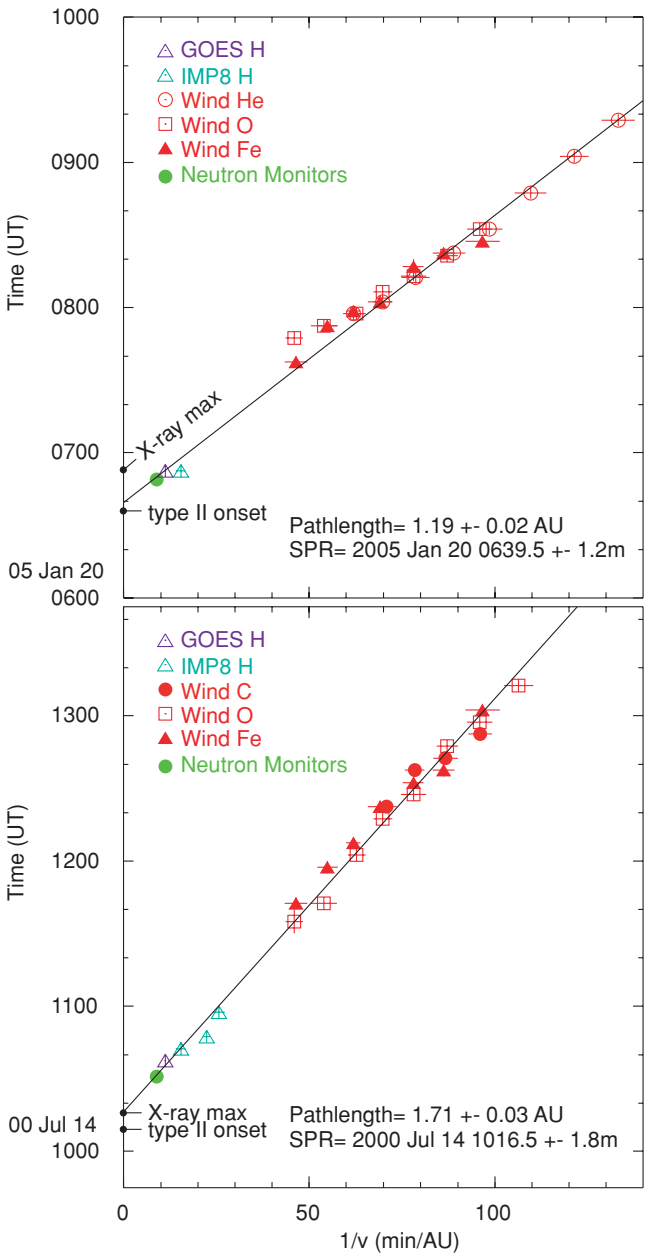

Figure 8. Onset times are plotted against inverse velocity for various energy intervals of listed species. The upper panel is for the large GLE event of 2005 January 20 and the lower is for the 2000 July 14, the Bastille Day event.

(A color version of this figure is available in the online journal.)

mentioned above. When the path length is long, e.g., $\sim$ 2 AU, the low-energy particles may take $\sim$ 4–5 hr to arrive. However, the magnetic field configurations typically remain stable for $\sim$ 2 hr on average. This may explain some of the wavering about the fit line for the event of 1998 August 24 shown in Figure 9. We suspect that these variations would be magnified for path lengths much greater than $\sim$ 2 AU, and, in addition, multiple scattering might also become an increasing delay factor.

For a spatially distributed source, changing flux tubes would be expected to have less effect on the progression of onset times than for a point source. In fact, impulsive sources have been observed to turn completely on and off as different energies arrive when observers cross magnetic flux tubes that are connected or not connected to the localized source (Mazur et al. 2000). For extended sources, intensities may vary somewhat but a connection persists. Changing direction and strength of the magnetic field accompanies the changing He intensities in the 2001 April 18 event shown in Figure 5. These different flux tubes may connect to different points along the shock. However, the regular progression of the He onset times tells us that the magnetic path length remains essentially constant.

The effect of pitch-angle scattering on onset times was modeled in some detail by Sáiz et al. (2005). By their criteria, most of our events fall nearest the "low threshold" category where the pre-event background is $\leqslant$ 0.01% of the peak intensity. Fortunately, the particles that arrive first have been scattered least. In this case, only $\sim$ 0.01% of the particles need arrive with minimal scattering for an accurate onset time to be determined; this is not a very demanding condition. Increasing thresholds intercept the intensity profile in a more slowly rising

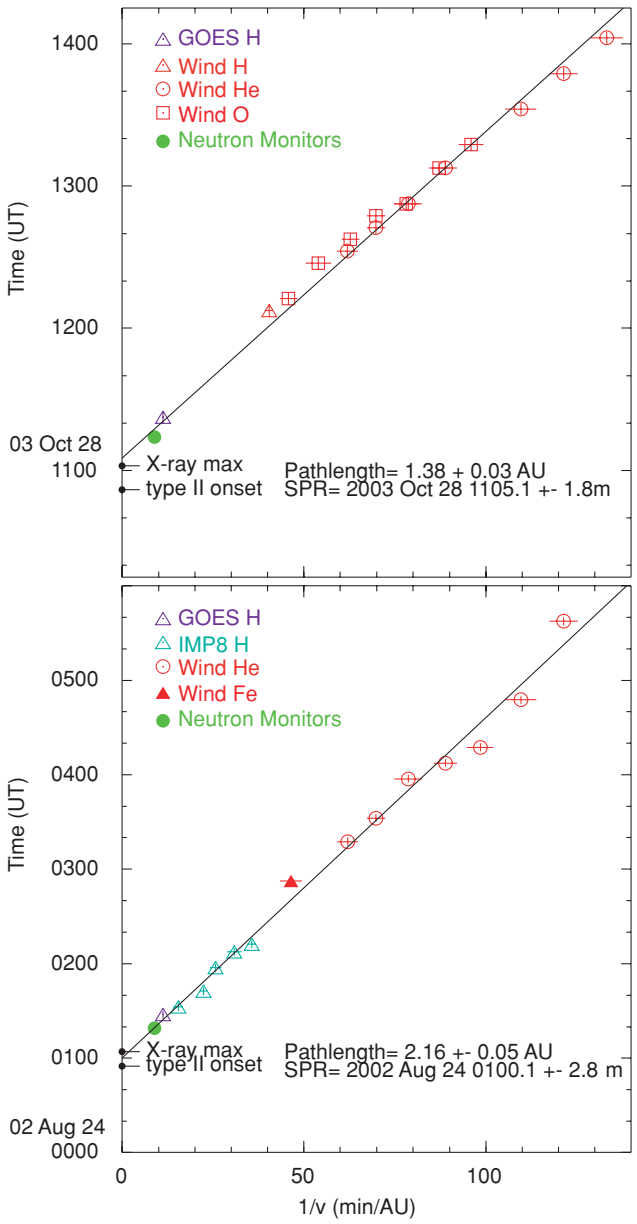

Figure 9. Onset times are plotted against inverse velocity for various energy intervals of listed species. The upper panel is for the GLE event of 2003 October 28 and the lower for the 2002 August 24.

(A color version of this figure is available in the online journal.)

region nearer peak intensity, causing later apparent onset times. In fact, however, this effect may not be as large as this model predicts. We consider the following three examples: (1) In the 2005 January 20 event (Figure 2), onsets for He with a threshold only ~ 10% of peak intensity are not significantly different from those for Fe, which vary between ~ 0.2% and ~ 1% of peak intensity. (2) The event with the longest path length, 2.16 AU, is the event of 2002 August 24. The proton intensities for this event, shown in Figure 6, rise rapidly from a threshold of ~ 0.1% of peak intensity, just as they do in many events with much smaller path lengths. We find it hard to believe that scattering contributes significantly to the observed sequence of delays for the protons and to the long path length for this event. (3) Finally, we have no idea how any model could treat the complex behavior of the event of 2001 April 18 shown in Figure 5.

The model used by Sáiz et al. (2005) assumes that the scattering parameters do not change with time throughout an event.

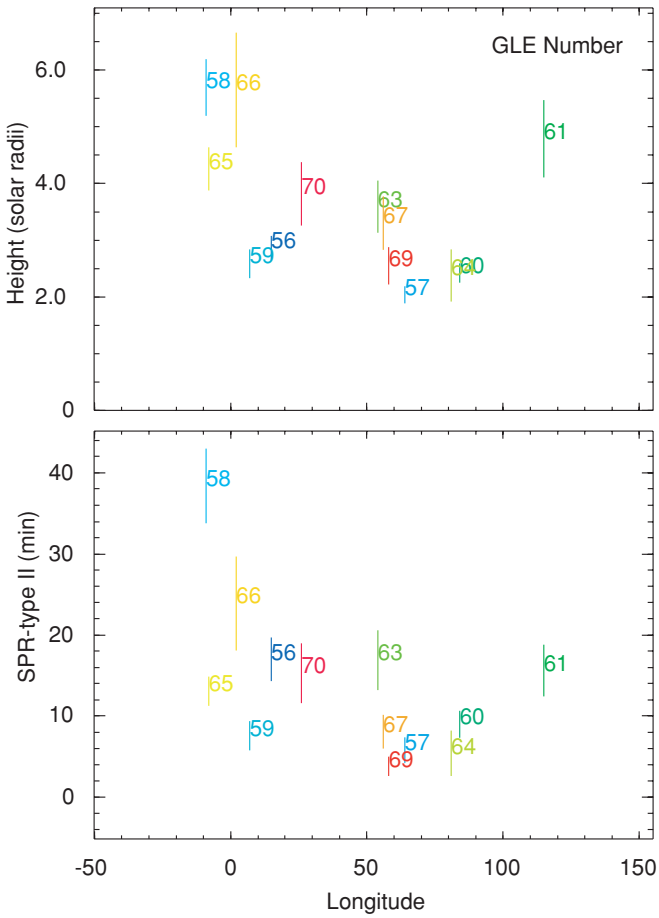

Figure 10. SPR time is shown as a function of the source longitude in the lower panel, while the upper panel shows the radial height of the shock at the time of first SPR vs. longitude (see text). Points are identified by their GLE number.

(A color version of this figure is available in the online journal.)

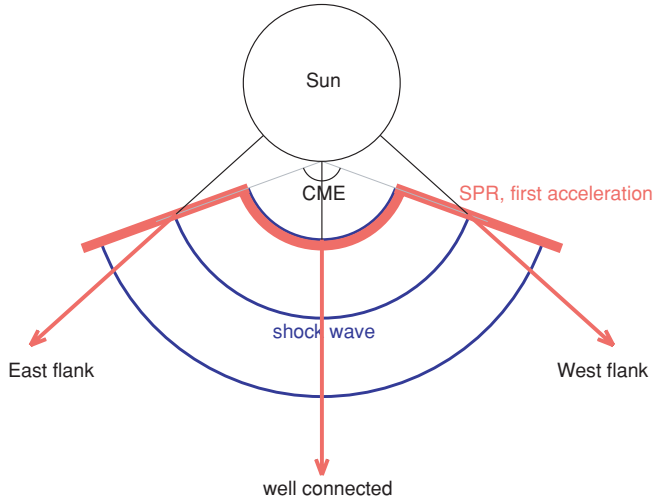

Figure 11. Possible acceleration scenario is shown in cartoon. Near the Sun, the ambient magnetic field lines (black) are radial. A shock wave (blue) forms over the central angles when, at ~ 1.5 R_S, the CME speed exceeds the local Alfvén speed. Acceleration begins (red region) at 2–4 R_S centrally or at higher altitudes at the flanks when the CME and shock expand laterally.

(A color version of this figure is available in the online journal.)

However, the particles streaming outward early in an event eventually reach sufficient intensities to significantly amplify Alfvén waves that increase the scattering of subsequent particles (see,

e.g., Ng et al. 2003). This means the earliest particles, that determine onsets, are scattered much less than those coming later that determine the intensity peak and subsequent decline. It is the shape of the peak and decay phase that is often used to determine "typical" scattering parameters for an event. While the possible effects of scattering should not be dismissed entirely, we believe that they do not greatly affect path lengths or SPR times, nor do they destroy the utility of SPR analysis or significantly alter our conclusions.

The best evidence that the SPR time is not systematically altered by scattering or other effects comes from the study of impulsive events by Tylka et al. (2003). These authors found SPR times that corresponded, as expected, with sharp peaks in hard X-ray intensities within errors of only 1–2 minutes.

The height versus time information for CMEs is usually based on a few widely spaced points in the low corona. Our assumption that the height increases linearly with time above 1.5 R_S usually agrees with CME height–time data within the quoted errors. As an example, in the 2005 January 20 event, the quadratic expression for the CME height versus time given by Gopalswamy et al. (2005) gives the height at our SRT of 3.0 $\pm$ 0.2 R_S, while our algorithm gives 2.6 $\pm$ 0.4 R_S. We have determined the radius at the SPR time using second-order fits to the CME height versus time data (http://cdaw.gsfc.nasa.gov/CME_list/) for 12 of our events. Of these, nine are within errors of the radii given in Table 1. However, the height–time measurements can often be $\sim$ 30 minutes to $\sim$ 1 hr apart, and we must often extrapolate the fit to obtain a height at the SPR time. In one extreme case (2000 July 14), this yields a nonphysical height of 0.4 R_S. Nevertheless, both techniques give a mean radius at SPR time of 2.7 R_S. Differences in the systematics of approximations and techniques do not alter the conclusions of this paper. Within an error of $\sim$ 0.5 R_S, our simple algorithm for height versus time has the advantage that it can be extended to historic GLE event where CMEs are not observed. We intend to employ this advantage in future work.

On the whole, we are pleased that we have been able to find consistent results for many of the GLE events in cycle 23. This suggests that the beginning of particle acceleration is a well-defined event, that particles are sufficiently numerous that a measurable number propagate near zero pitch angle along field lines with minimal scattering, and that the important properties of magnetic flux tubes frequently persist for several hours.

6. CONCLUSIONS

Using onset times for various ions of different velocities, we have been able to determine the initial solar particle release times and magnetic path lengths for 13 of the 16 GLE events in solar cycle 23. We can draw the following conclusions:

1. Magnetic path lengths from the Sun to Earth vary by a factor up to $\sim$ 2 from event to event. In most events, the same paths are traversed by all species and energies and the path lengths are well determined.
2. The initial solar particle release times occur after the onset times of type II emission in all events.
3. The onset of acceleration is a well-defined occurrence, independent of particle species and energy, on any arbitrary source longitude that we have studied over the span of $\sim$ 125°. SPR times for poorly connected events are as well defined as for well-connected events.
4. As a specific consequence of (3), we see no evidence that high-speed or high-rigidity particles reach distant longitudes from the source at earlier times, for example. This argues that the ions do not cross field lines or move laterally across the corona on their trajectory. It also favors a source that is spatially distributed in longitude, like a shock wave.
5. When we interpret the SPR time in terms of a height of initial acceleration in the corona, the pattern of height versus longitude is consistent with shock acceleration.

We thank Nand Lal and Bryant Heikkila for their assistance in obtaining 5-minutes averaged data from *IMP-8*. We also thank Ed Cliver, Frank McDonald, Chee Ng, and Allan Tylka for helpful discussions and for their comments on the manuscript. This work was funded by NASA grant NNX08AQ02G.

REFERENCES

Bieber, J. W., et al. 2005a, Proc. 29th Int. Cosmic Ray Conf. (Pune) Vol 1, 237
Bieber, J. W., Clem, J., Evenson, P., Pyle, R., Ruffolo, D., & Sáiz, A. 2005b, GRL 32, L03S02 doi:10.1029/2004GL021492
Bieber, J. W., et al. 2002, ApJ, 567, 622
Cliver, E. W. 2006, ApJ, 639, 1206
Cliver, E. W., & Ling, A. G. 2007, ApJ, 658, 1349
Cliver, E. W., Kahler, S. W., & Reames, D. V. 2004, ApJ, 605, 902
Cliver, E. W., Kahler, S. W., Shea, M. A., & Smart, D. F. 1982, ApJ, 260, 362
Cliver, E. W., Nitta, N. V., Thompson, B. J., & Zhang, J. 2005, Sol. Phys., 225, 105
Desai, M. I., Mason, G. M., Mazur, J. E., Dwyer, J. R., Gold, R. E., Krimigis, S. M., Smith, C. W., & Skoug, R. M. 2003, ApJ, 588, 1149
Fisk, L. A. 1978, ApJ, 224, 1048
Flückiger, E. O., Bütikofer, R., Moser, M. R., & Desorgher, L. 2005, Proc. 29th Int. Cosmic Ray Conf. (Pune), 1, 225
Gopalswamy, N., Lara, A., Kaiser, M. L., & Bougeret, M. L. 2001, J. Geophys. Res., 106, 25261
Gopalswamy, N., Xie, H., Yashiro, S., & Usoskin, I. 2005, Proc. 29th Int. Cosmic Ray Conf. (Pune), 1, 169
Gosling, J. T. 1993, J. Geophys. Res., 98, 18937
Kahler, S. W. 1992, ARA&A, 30, 113
Kahler, S. W. 1994, ApJ, 428, 837
Kahler, S. W. 2001, J. Geophys. Res., 106, 20947
Krucker, S., Larson, D. E., Lin, R. P., & Thompson, B. J. 1999, ApJ, 519, 864
Larson, D. E., et al. 1997, GRL, 24, 1911
Lee, M. A. 1983, J. Geophys. Res., 88, 6109
Lee, M. A. 1997, in Coronal Mass Ejections, ed. N. Crooker, J. A. Jocelyn, & J. Feynman, Geophys. Monograph 99 (Washington, DC: AGU Press), 227
Lee, M. A. 2005, ApJ, 158, 38
Leske, R. A., Cummings, J. R., Mewaldt, R. A., Stone, E. C., & von Rosenvinge, T. T. 1995, ApJ, 452, L149
Lin, R. P., Potter, D. W., Gurnett, D. A., & Scarf, F. L. 1981, ApJ, 251, 364
Mann, G., Aurass, H., Klassen, A., Estel, C., & Thompson, B. J. 1999, in Plasma Dynamics and Diagnostics in the Solar Transition Region and Corona, ed. J.-C. Vial & B. Kaldeich-Schurmann (ESA SP-446; Noordwijk: ESA), 477
Mann, G., Klassen, A., Aurass, H., & Classen, H. T. 2003, A&A, 400, 329
Mason, G. M., Mazur, J. E., & Dwyer, J. R. 1999, ApJ, 525, L133
Mazur, J. E., Mason, G. M., Dwyer, J. R., Giacalone, J., Jokipii, J. R., & Stone, E. C 2000, ApJ, 532, L79
McGuire, R. E., von Rosenvinge, T. T., & McDonald, F. B. 1986, ApJ, 301, 938
Meyer, J. P. 1985, ApJS, 57, 151
Miller, J. A. 1998, Space Sci. Rev., 86, 79
Miller, J. A., & Viñas, A. F. 1993, ApJ, 412, 386
Moraal, H., McCracken, K. G., Schoemana, C. C., & Stoker, P. H. 2005, Proc. 29th Int. Cosmic Ray Conf. (Pune), 1, 221
Ng, C. K., Reames, D. V., & Tylka, A. J. 2003, ApJ, 591, 461
Nitta, N. V., Reames, D. V., DeRosa, M. L., Liu, Y., Yashiro, S., & Gopalswamy, N. 2006, ApJ, 650, 438
Ramaty, R., Mandzhavidze, N., & Kozlovsky, B. 1996, in High Energy Solar Physics, ed. R. Ramaty, N. Mandzhavidze, & X.-M. Hua, AIP Conf. Proc Vol 374 (Woodbury, NY: AIP Press), 172

Reames, D. V. 1990, ApJS, 73, 235
Reames, D. V. 1995, Revs. Geophys. (Suppl.), 33, 585
Reames, D. V. 1999, Space Sci. Rev., 90, 413
Reames, D. V. 2000, ApJ, 540, L111
Reames, D. V. 2002, ApJ, 571, L63
Reames, D. V., Barbier, L. M., von Rosenvinge, T. T., Mason, G. M., Mazur, J. E., & Dwyer, J. R. 1997, ApJ, 483, 515
Reames, D. V., & Ng, C. K. 2004, ApJ, 610, 510
Reames, D. V., Ng, C. K., & Berdichevsky, D. 2001, ApJ, 550, 1064
Reames, D. V., & Stone, R. G. 1986, ApJ, 308, 902
Reames, D. V., von Rosenvinge, T. T., & Lin, R. P. 1985, ApJ
Roth, I., & Temerin, M. 1997, ApJ, 477, 940
Ruffolo, D. 1997, ApJ, 481, L119
Sáiz, A., Evenson, P., Ruffolo, D., & Bieber, J. W. 2005, ApJ, 626, 1131
Simnett, G. M., & Roelof, E. C. 2005, Proc. 29th Int. Cosmic Ray Conf. (Pune), 1, 233
Temerin, M., & Roth, I. 1992, ApJ, 391, L105
Tylka, A. J. 2001, J. Geophys Res., 106, 25333
Tylka, A. J., Boberg, P. R., Adams, J. H., Jr., Beahm, L. P., Dietrich, W. F., & Kleis, T. 1995, ApJ, 444, L109
Tylka, A. J., Cohen, C. M. S., Deitrich, W. F., Maclennan, C. G., McGuire, R. E., Ng, C. K., & Reames, D. V. 2001, ApJ, 558, L59
Tylka, A. J., et al. 2003, Proc. 28th Int. Cosmic Ray Conf., 3305
Tylka, A. J., Cohen, C. M. S., Dietrich, W. F., Lee, M. A., Maclennan, C. G., Mewaldt, R. A., Ng, C. K., & Reames, D. V. 2005, ApJ, 625, 474
Tylka, A. J., & Lee, M. A. 2006, ApJ, 646, 1319
von Rosenvinge, T. T., et al. 1995, Space Sci. Rev., 71, 155
Vršnak, B., Magdalenić, J., Aurass, H., & Mann, G. 2002, A&A, 396, 673